EPJ Web of Conferences **95**, 05004 (2015)
DOI: 10.1051/epjconf/ 20159505004

Generation of higher flow harmonics in Pb+Pb collisions at LHC in HYDJET++ model

B. H. Brusheim Johansson[1,a], L. V. Bravina[1,b], G. Kh. Eyyubova[2,c], V. L. Khoroktikh[2,d], I. P. Lokhtin[2,e], L. V. Malinina[2,f], S. P. Petrushanko[2,g], A. M. Snigirev[2,h] and E. E. Zabrodin[1,2,i]

[1] *Department of Physics, University of Oslo, Pb. 1048 Blindern, N-0316 Oslo, Norway*
[2] *Skobeltsyn Institute of Nuclear Physics Lomonosov Moscow State University, RU-119991 Moscow, Russia*

Abstract. The influence of elliptic and triangular flow on higher flow harmonics is studied within the HYDJET++ model, which merges parametrized hydro with jet quenching. Even harmonics can be generated by elliptic flow only, while odd harmonics need non-zero triangular component. A hydrodynamical model predicts a scaling of v_4/v_2^2 ratio with p_T , while jets force a rise of the high p_T tail of the ratio. Hexagonal flow appears to be an interesting interplay between v_2 and v_3. It shows a dominant contribution of v_3 in central events and v_2 at more peripheral collisions. Comparison with ALICE, ATLAS and CMS experimental data is presented.

1 Introduction

An objective of the Heavy Ion Program at e.g. RHIC and LHC experiments is to examine the properties of new states of matter. The first findings pointing in the direction of a perfect fluid were made at RHIC collider [1–4]. Since then, the view upon the initial prehadronic state shifted towards the fluid/plasma view from the ideal gas picture [5]. The new paradigm is investigated through a few common observables. One observable is the particle spectra, which allows for investigation of prehadronic matter and also aspects of hadronic genesis. A common observable connected to the particle spectra is R_{AA}, i.e. the number cross section modification factor. This observable is a feature of the matter in the collisions and points to the above stated fluid/plasma picture, quantifying the deviation from *in vacuo* hadronic genesis. The properties and dynamics of matter are also accessible through other observables such as anisotropic flow harmonics [6]. Since heavy ion collision phenomena involve jet production, the need to describe heavy ion collisions as a combination of soft *and* hard physics is obvious. The focus of present paper is the work and progress in calculating spectra and

[a] e-mail: bhjohan@uio.no
[b] e-mail: larissa.bravina@fys.uio.no
[c] e-mail: eyyubova@mail.cern.ch
[d] e-mail: vlk@lav1.npi.msu.su
[e] e-mail: Lokhtin@cern.ch
[f] e-mail: malinina@lav01.sinp.msu.ru
[g] e-mail: petrushanko@lav01.sinp.msu.ru
[h] e-mail: snigirev@lav.npi.msu.su
[i] e-mail: Zabrodin@fys.uio.no

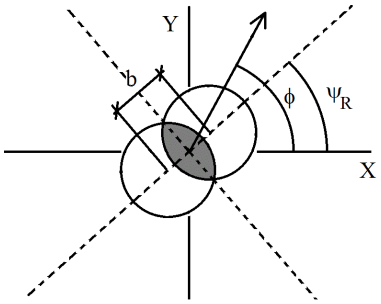

Figure 1. Identification of reaction plane, impact parameter and azimuth.

flow of hadrons in relativistic heavy ion collisions, including jets in the model. The main goal is to reproduce the spectra for identified particles i.e. pions, kaons and protons together with the calculation of flow harmonics. The HYDJET++ model provides us with an array of possibilities in investigating possible mechanisms related to heavy ion collisions. The analysis of flow is based on the Fourier series expansion of the invariant particle distribution [7, 8]

$$E\frac{d^3N}{d^3p} = \frac{1}{\pi}\frac{d^2N}{dp_T^2 dy}\left[1 + 2\sum_{n=1}^{\infty} v_n \cos n(\phi - \Psi_n)\right]. \tag{1}$$

Here, the ϕ is the azimuth of the particle momentum and the participant event plane is denoted by Ψ_n (Fig.1). The transverse momentum is denoted p_T and the particle rapidity is referred to as y. The flow harmonic coefficients

$$v_n = \langle \cos n(\phi - \Psi_n) \rangle \tag{2}$$

are obtained by averaging over all events. The directed (v_1) and elliptic (v_2) flow has been studied for the last decades and are common observables [9, 10] when studying prehadronic matter and hadron genesis. The investigation of higher harmonics started more recently and is maturing at present.

The investigation of the second and third harmonics is the base of the flow programme. The initial matter distribution has an elliptic shape and thus possess an even type of symmetry. This means that to a first approximation, the odd harmonics will vanish. Further, the higher harmonics will be more dependent on fluctuations in the matter and they will also be dependent in a more non-trivial way than lower order harmonics. The knowledge of higher harmonics is maturing and the relation of different types of harmonics is starting to be examined. In present paper, these dependences of higher harmonics will be examined within the HYDJET++ model.

2 The HYDJET++ Model

The heavy ion simulation package HYDJET++ [11] is based on the Monte Carlo event generators FAST MC [12], and PYQUEN [13]. The FAST MC code generates soft hadronic states on the chemical and thermal hyper surfaces of the produced matter distribution originating from heavy ion collisions. The model involves parameterized hydrodynamics with preset parameters. The code generates the kinematics and the hadronic resonances with following decays.

In the PYQUEN model, the jet quenching effect is modeled with radiative and collisional energy loss in a matter distribution with size L. The partonic radiative energy loss (Fig.2(a)) is modeled within

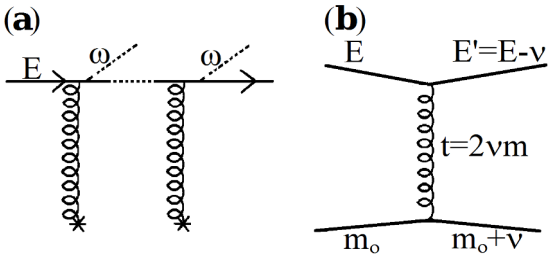

Figure 2. Radiation in BDMS framework (a). Parton traversing media radiating gluons [14, 15]. Collision in high momentum limit [13, 16] (b).

the BDMS framework [14, 15]. The scattering and thus the gluon mean free path (λ_g) is characterized by the transport coefficient $\hat{q} = \mu_D^2/\lambda_g$. The *in medio* gluon spectra is represented as

$$\frac{\omega dI}{d\omega dz} = \frac{2\alpha_s C_R}{\pi L}\left[1 - y + \frac{y^2}{2}\right] \ln|\cos(\omega_1 \tau_1)|, \tag{3}$$

where

$$\omega_1 = \sqrt{i\left(1 - y + \frac{C_R}{3}y^2\right)\bar{\kappa}\ln(\frac{16}{\bar{\kappa}})}, \quad \bar{\kappa} = \frac{\mu_D^2 \lambda_g}{\omega\,(1-y)}, \quad \tau_1 = L/(2\lambda_g). \tag{4}$$

Here, α_s is the running coupling, the color factor $C_R = 4/3$ and $y = \omega/E$, where E and ω denotes the parton and gluon energy. The Debye screening mass μ_D squared is here equal to the minimum momentum transfer t_{min}.

The partonic collisional energy loss (Fig. 2(b)) is generically calculated in the high momentum limit with temperature T as [13, 16]

$$\frac{dE}{dl} = \frac{1}{4T\lambda\sigma}\int_{\mu_D^2}^{t_{max}} dt \frac{d\sigma}{dt} t, \tag{5}$$

with cross section σ and mean free path λ.

The soft "thermal" states are generated from the co-variant, partially equilibrated distribution, which is a function of mass, strangeness suppression, chemical freeze-out temperature, hadronic potential and also spin degeneracy. The freeze-out temperature is parameterized in terms of collision energy ($\sqrt{s}$). The particle multiplicity is then calculated on the chemical freeze-out hyper surface. The produced particles will then obey a Poisson distribution.

In the model, a linear rapidity profile is used. This gives the relation between the transverse rapidity $\tilde{\rho}_u$ and the matter radius r as

$$\tilde{\rho}_u = \frac{r}{R_f\,(b)}\rho_u^{max}\,(b=0)\,, \tag{6}$$

where the individual event planes are used as a part of the rapidity modulation or, equivalently, the rms emission radius R_f. For present article the rapidity parameterization

$$\rho = \rho_0 \left[1 + \rho_3 \cos(3(\Psi_3 - \phi)) \right] \tag{7}$$

is used. The new event plane for the triangular flow is uncorrelated to the model "reaction plane" and is uniformly randomly distributed. The transverse radius of the fireball is then calculated with the spatial anisotropy parameter $\epsilon(b)$ and the mean emission radius $R_f(b)$ as

$$R(b, \phi) = R_f(b) \frac{\sqrt{1 - \epsilon^2(b)}}{\sqrt{1 + \epsilon(b) \cos(2\phi)}}. \tag{8}$$

The effective volume is calculated in the same manner, using the mean particle multiplicity as weight.

For the hard part, the mean number of jets is proportional to the number of inelastic in-matter collisions. When shadowing S is accounted for, the mean multiplicity is calculated as

$$\bar{N}^{jet} = \int_{min(hard)} dp_T^2 \int dy \frac{d\sigma^{hard}\left(p_T, \sqrt{s}\right)}{dp_T^2 dy} \int_0^{2\pi} d\Psi \int_0^{\infty} drrT_A(r_1) T_A(r_2) S(r_1, r_2, p_T, y). \tag{9}$$

The shadowing $S \leq 1$ is likely significant at LHC energies. This effect stems from interference between the target and projectile.

3 Effect of Jets on v_4/v_2^2

The calculation of the higher harmonics ($n > 3$) within HYDJET++ is done in [17]. Developing the code and the algorithms has transformed into an activity characterized by investigation of flow and spectra analysis. As one of the first attempts of a more sophisticated analysis, the investigation of the consequences of incorporating jets in the calculations [18, 19] is carried out. The theoretical hydrodynamics prediction of $v_4/v_2^2 = 0.5$ [20] is compared to calculations which incorporates jets. Experiments reveal a value of $v_4/v_2^2 \sim 1$ [21, 22]. Different modes of particle genesis are examined using the projection features of the HYDJET++. The elliptic and quadrangular flow are calculated for hydro-dynamically produced particles, jet produced particles and also for directly produced particles. The fourth order event-plane (Ψ_4) is not generated in the present version, so the quadrangular flow is projected onto the second order event plane. This should be taken into consideration when evaluating the calculations since the actual Ψ_2 and Ψ_4 planes do not necessarily coincide. Also, event-by-event fluctuations should increase the ratio if present. To compensate for these types of fluctuations we impose a Knudsen-type of parameter [23, 24].

Both elliptic and quadrangular flow are reproduced out to $p_T \sim 2$ GeV/c. Although the qualitative features of the elliptic flow are reproduced, the ratio is not quantitatively reproduced for a lower energy/mass setting (Fig.3) [18, 19]. This deviation likely stems from the model specific description of initial conditions. Quenched jets are shown to increase the ratio over the whole p_T range. Adding event-by-event fluctuations to the HYDJET++ model provides us with a quantitaive model of the ratio. Also, the high p_T tail is not believed to be reproduced without jet production included in the simulations.

4 Hexagonal Flow as a Superposition of Ellipticity and Triangularity

Next, we examine the hypothesis of higher harmonics as a superposition of lower, i.e. elliptic and triangular flow.

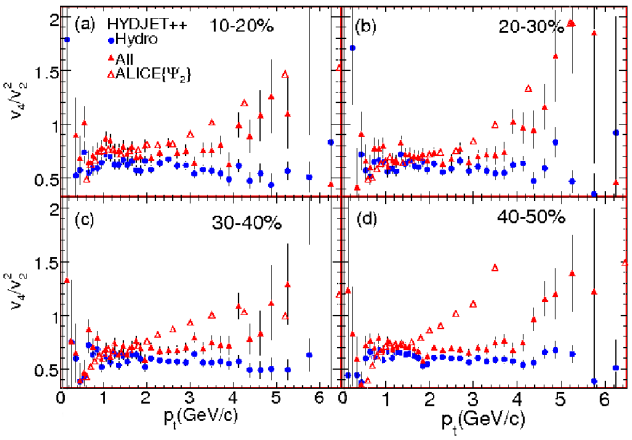

Figure 3. Ratio v_4/v_2^2: Calculations are compared to experimental data [22].

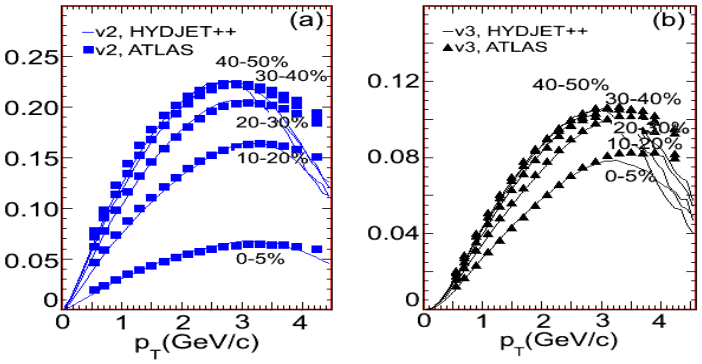

Figure 4. Elliptic (a) and triangular flow (b) calculated for five centralities: 0-5%, 10-20%, 20-30%, 30-40% and 40-50%. Experimental data are taken from [26].

The HYDJET++ is tuned to reproduce the elliptic and triangular flow (Fig.4) to a high degree of accuracy. In addition, calculated spectra of identified particles nicely coincide with the experimental data (Fig.5) although the antiproton spectra are seen to deviate from simulations. This deviation might be due to rescattering in the later stages of collisions [27].

The setting used here in calculating higher harmonics is somewhat incomplete yet interesting: The hexagonal flow is projected onto the second and third (Ψ_2, Ψ_3) event plane and the fireball deformation is only modeled in terms of triangularity and ellipticity.

The hexagonal flow in the second event plane increases monotonically with centrality, not displaying the limiting behaviour of experimental data [28]. The correlation with the second event plane is mainly in the lower p_T (Fig.6) and centrality range. For higher p_T, the interference from the model Ψ_3 plane is visible (Fig.7). The projection of the hexagonal flow onto the third event plane also displays

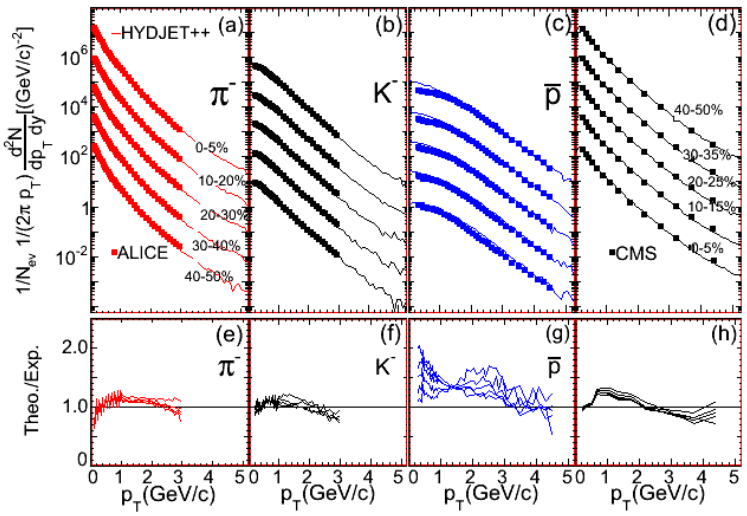

Figure 5. Identified particle spectra compared to ALICE spectra [29] (ratio) for π^-(a), K^-(b) and $\bar{p}$(c). Particle spectra for CMS [30].

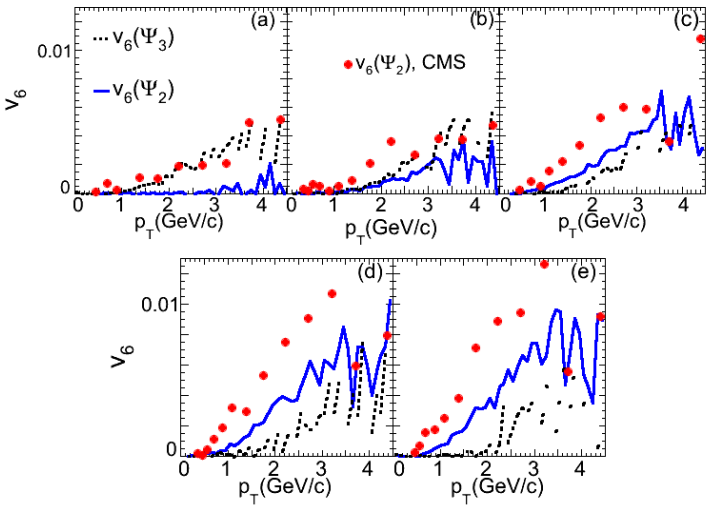

Figure 6. Hexagonal flow. $v_6(p_T)$ is projected onto the second and third event planes. The panel centralities are: 0 – 5%(a), 10 – 20%(b), 20 – 30%(c), 30 – 40%(d) and 40 – 50%(e) Data are included for qualitative comparison [28] (CMS).

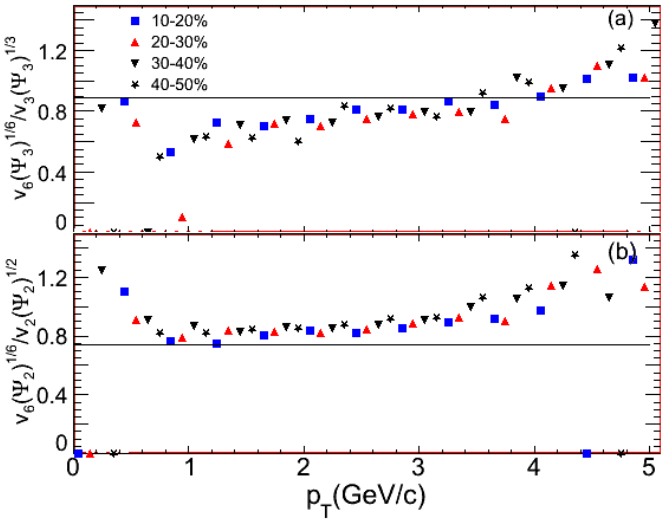

Figure 7. Ratio $v_6^{1/6}/v_3^{1/3}$ (a) and $v_6^{1/6}/v_2^{1/2}$ (b). Hexagonal flow projected onto model second and third event plane. Hydrodynamical predictions are included for relation to elliptic and triangular flow: $v_6^{1/6}/v_2^{1/2} = (1/6)^{1/6} \approx 0.74$, $v_6^{1/6}/v_3^{1/3} = (1/2)^{1/6} \approx 0.89$. Four different centralities are displayed: $10-20\%$, $20-30\%$, $30-40\%$ and $40-50\%$.

a correlation with the triangular flow (Fig.6). This correlation is at its strongest for higher p_T (Fig.7) and centrality range. The Ψ_3 projection also interferes with the second event plane for lower p_T.

5 Discussion

The work on the HYDJET++ model has progressed to a level where analysis with a certain degree of complexity has become feasible. The calculation of particle spectra and lower harmonics is done with a high degree of accuracy. The higher harmonics remain to be reproduced quantitatively due to missing eventplanes.

The inclusion of jets in the calculations has proved valuable, in particular adding to the qualitative feature of the high p_T relation between the second and fourth order harmonics [18, 19]. This investigation provides new insights of jet phenomena.

The investigation of the hypothesis of ellipticity and triangularity as the only geometric modes provides us with new insights of anisotropy genesis. The hexagonal flow is seen to be qualitatively reproduced by these two fundamental modes [25]. However, the quantitative results deviate from experimental data. The influence of higher order deformations in the experimental data are a possible source of deviation from our calculations due to the restriction of only implementing second and third eventplane in the model. This feature can be examined further. Due to the setting stated, the calculated hexagonal flow is expected to deviate from the experimentally obtained flow, however a "tracking" of the calculated flow would at least give us a hint of the amount of v_6-eccentricity needed with the present ellipticity and triangularity [31]. This "lost flow" might then be accounted to higher order deformations (4,5 ...).

References

[1] I. Arsene *et al.* (BRAHMS Collaboration), Nucl. Phys. A **757**, 1 (2005).
[2] B. B. Back *et al.* (PHOBOS Collaboration), Nucl. Phys. A **757**, 28 (2005).
[3] J. Adams *et al.* (STAR Collaboration), Nucl. Phys. A **757**, 102 (2005).
[4] K. Adcox *et al.* (PHENIX Collaboration), Nucl. Phys. A **757**, 184 (2005).
[5] E. Shuryak, Prog. Part. Nucl. Phys. **53**, 273 (2004).
[6] J.-Y. Ollitrault, Phys. Rev. D **46**, 229 (1992).
[7] S. Voloshin and Y. Zhang, Z. Phys. C **70**, 665 (1996).
[8] A. M. Poskanzer and S. A. Voloshin, Phys. Rev. C **58**, 1671 (1998).
[9] B. Alver *et al.*, Phys. Rev. Lett. **98**, 242302 (2007).
[10] S. A. Voloshin, A. M. Poskanzer, in *Relativistic Heavy Ion Physics*, Landolt-Börnstein DataBase, Vol. 23 ed. by R. Stock (Springer, Berlin, 2010), p.5-54.
[11] I. P. Lokhtin *et al.*, Comp. Phys. Comm. **180**, 779 (2009).
[12] N. S. Amelin *et al.*, Phys. Rev. C **74**, 064901 (2006); *ibid.* **77**, 014903 (2008).
[13] I. P. Lokhtin and A. M. Snigirev, Eur. Phys. J. C **16**, 527 (2000).
[14] R. Baier *et al.*, Nucl. Phys. B **483**, 291 (1997); *ibid.* **484**, 265 (1997).
[15] R. Baier, Yu. L. Dokshitzer, A. H. Mueller and D. Schiff, Nucl. Phys. B **531**, 403 (1998).
[16] E. Braaten and M. H. Thoma, Phys. Rev. D **44**, 1298 (1991).
[17] L. V. Bravina *et al.*, Eur. Phys. J. C **74**, 2807 (2014).
[18] E. Zabrodin *et al.*, Acta Phys. Polon. B Proc. Supp. **5**, 349 (2012).
[19] L. Bravina *et al.*, Phys. Rev. C **87**, 034901 (2013).
[20] N. Borghini and J.-Y. Ollitrault, Phys. Lett. B **642**, 227 (2006).
[21] A. Adare *et al.* (PHENIX Collaboration), Phys. Rev. Lett. **105**, 062301 (2010).
[22] B. Abelev *et al.* (ALICE Collaboration), CERN-PH-EP-2012-142 (unpublished).
[23] C. Gombeaud, and J.-Y. Ollitrault, Phys. Rev. C **81**, 014901 (2010).
[24] M. Luzum, C. Gombaud and J.-Y. Ollitrault, Phys. Rev. C **81**, 054910 (2010).
[25] L. Bravina, *et al.*, Phys. Rev. C **89**, 024909 (2014).
[26] G. Aad, *et al.* (ATLAS Collaboration), CERN-PH-EP-2012-035.
[27] F. Becattini, *et al.*, arXiv 1405.0710v3 (2014).
[28] S. Chatrchyan *et al.* (CMS Collaboration), Phys. Rev. C **89**, 044906 (2014).
[29] B. Abelev *et al.* (ALICE Collaboration), CERN-PH-EP-2013-019.
[30] S. Chatrchyan *et al.* (CMS Collaboration), Phys. Rev. C **87**, 014902 (2013).
[31] R. A. Lacey *et al.*, Phys. Rev. C **83**, 044902 (2011).